WELDING RESEARCH

SUPPLEMENT TO THE *WELDING JOURNAL*, NOVEMBER 1995
Sponsored by the American Welding Society and the Welding Research Council

Surface Temperature Distribution of GTA Weld Pools on Thin-Plate 304 Stainless Steel

Variations in weld pool surface tension appear to control fluid flow and heat transfer

BY T. ZACHARIA, S. A. DAVID, J. M. VITEK AND H. G. KRAUS

ABSTRACT. A transient multidimensional computational model was utilized to study gas tungsten arc (GTA) welding of thin-plate 304 stainless steel (SS). The model eliminates several of the earlier restrictive assumptions including temperature-independent thermal-physical properties. Consequently, all important thermal-physical properties were considered as temperature dependent throughout the range of temperatures experienced by the weld metal. The computational model was used to predict surface temperature distribution of the GTA weld pools in 1.5-mm-thick AISI 304 SS. The welding parameters were chosen so as to correspond with an earlier experimental study that produced high-resolution surface temperature maps. One of the motivations of the present study was to verify the predictive capability of the computational model. Comparison of the numerical predictions and experimental observations indicate excellent agreement, thereby verifying the model.

Introduction

During welding, the development of the weld pool is determined by the arc-metal interaction, heat flow and fluid flow, the thermophysical properties of the material and the associated boundary conditions. There have been a number of theoretical studies of welding in order to understand the underlying mechanism that controls the development of the weld bead and its properties (Refs. 1–19). The influence of heat flow and fluid flow and their effect on the weld pool shape is well documented (Refs. 8–19). Besides the information on weld pool shape and size, computational modeling of welding can provide detailed information on such parameters as weld cooling rate, temperature gradient in the weld pool and macroscopic growth rate.

Initial attempts at studying the effects of heat flow in welding concentrated on the development of analytical solutions (Ref. 1) or semi-empirical expressions (Ref. 2) for the study of heat flow in the weldments. Rosenthal developed an analytical solution for moving heat sources and applied these solutions to arc welding operations (Ref. 1). Since then, there has been a number of attempts to study the effect of plate thickness on cooling rates, temperature distribution in a plate of finite thickness and the effect of cooling rate on the weld cross-sectional area. Even though these studies provided significant insight and had the advantage of simplicity, the applications of these solutions were fairly restrictive and could not be used for a generalized study of the welding operation.

More recently, there has been a number of studies which employed numerical techniques using finite difference, finite element or control volume approaches to study the transient heat flow and fluid flow phenomena that occur during welding (Refs. 8–19). Most authors have been concerned with the problem of heat and fluid flow during stationary GTA welding. The objective of these studies was to determine how the process parameters affected weld pool geometry. As a result of these studies, important physical insight into the mechanism of weld pool development was achieved. These studies demonstrated that, in most cases, the fluid flow and heat transfer in the weld pool is controlled by the spatial variation of surface tension that exists on the weld pool surface. The spatial variation of surface

KEY WORDS

Surface Temperature
Temperature Distribution
GTAW Pools
Thin-Plate 304 SS
Computational Model
Multidimensional
Heat Flow
Fluid Flow
Convection Heat Transfer
Model Verification

T. ZACHARIA, S. A. DAVID and J. M. VITEK are with the Metals and Ceramics Division, Oak Ridge National Laboratory, Oak Ridge, Tenn. H. G. KRAUS is with Idaho National Engineering Laboratory, EG&G Idaho, Inc., Idaho Falls, Idaho.

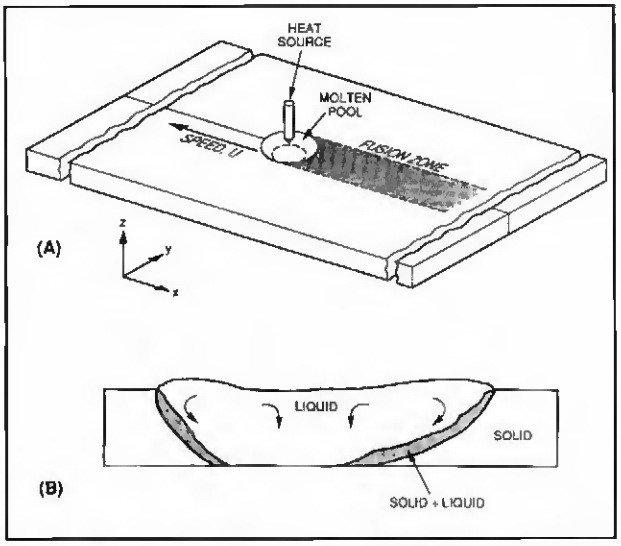

Fig. 1 — Schematic drawing of: A — the GTA welding process; B — the weld pool showing the region of interest.

tension causes the molten metal to be drawn along the surface from a region of lower surface tension to that of higher surface tension resulting in large surface flows. For pure metals and alloys, the temperature dependency of surface tension ($d\gamma/dT$) is negative, causing outward flow at the surface. On the other hand, surface active elements such as sulfur can produce a positive $d\gamma/dT$, resulting in an inward flow.

In previous investigations, the authors examined the detailed heat flow and fluid flow that occurred during stationary GTA welding of 304 SS (Refs. 15–18). These studies provided an improved understanding of the free surface effects and the surface tension gradient driven flow. The weld pool surface was treated as a free deformable surface. An improved understanding of the surface tension gradient effect was achieved by calculating $d\gamma/dT$ as a function of temperature and concentration of surface active elements (Ref. 20). It was shown that, depending on the material composition and welding conditions, the temperature coefficient of surface tension $d\gamma/dT$ may go through an inflection point, initially increasing before decreasing with temperature.

The change in $d\gamma/dT$ from a positive value at low temperature to a negative value at high temperature has important consequences on the weld pool fluid flow and heat transfer, and the ultimate development of the weld. Directly below the welding heat source, a hot zone exists where the temperature experienced by the molten weld metal is likely to be above the critical temperature such that a negative $d\gamma/dT$ prevails in this region. This would cause two opposing surface tension gradients existing on the weld pool surface: a positive surface tension gradient at the periphery of the weld pool and a negative surface tension gradient at the center of the weld pool. Depending on the relative magnitude of the two driving forces that the molten metal may encounter, either a radially outward flow or a radially inward flow, or even a combination of both resulting in two opposing vortices, may develop.

Even though most of the numerical studies of welding concentrated on stationary spot GTA welding, there have been some notable works on moving arc welds. The work of Kou, *et al.* (Ref. 12), Friedman (Ref. 3), Kraus (Ref. 14) and Zacharia, *et al.* (Ref. 15), are some examples of previous work on nonstationary heat sources. A review of the literature on the modeling of fundamental phenomena is presented in Ref. 21. In the present study, weld pool convective heat transfer has been solved in detail for full penetration welding of thin-plate 304 SS. Three-dimensional heat and fluid flow that occur during full-penetration linear GTA welding were numerically studied. The numerical results are compared with experimentally obtained values to evaluate the predictive capability of the model.

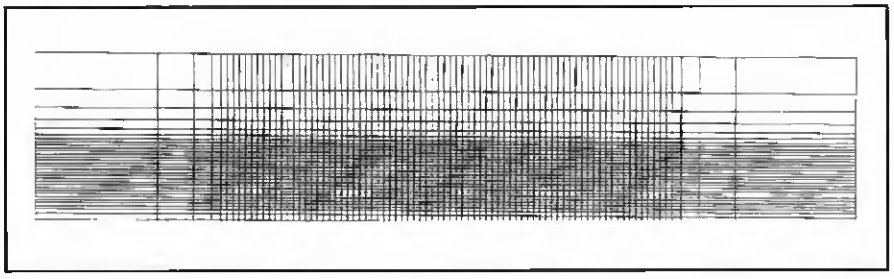

Fig. 2 — The grid system used for calculating weld pool heat and fluid flow.

Computatiooal Model

Figure 1 is a schematic diagram of the idealized welding process. The welding arc supplies thermal energy to the workpiece, via radiative, convective and electronic contributions, producing the weld pool. This weld pool follows the heat source as the welding arc is translated to produce the weld bead or the welded joint. The properties of the welded joint depend to a great extent on the various phenomena that occur within the weld pool. For example, the width and the depth of the weld bead depend on the balance between the convective heat transfer within the weld pool and the conductive heat transfer that occurs in the solid region. Flow in the pool is driven by a combination of buoyancy, electromagnetic and surface tension forces. The computational modeling effort requires consideration of the current and heat flux distribution due to the arc, interaction of the arc with the weld pool free surface, convective heat transfer due to fluid flow in the molten pool, heat of fusion and solidification, convective and radiative losses from the surface, and heat and mass loss due to vaporization.

The transient heat transfer problem of autogenous GTA welding of 304 SS plate was analyzed numerically using a transient, multidimensional computational model (Refs. 16, 18). Initially, the computational model was successfully applied to the solution of heat flow and fluid flow that occur during stationary GTA welding of 40 x 40 x 10-mm (1.6 x 1.6 x 0.4-in.) thick 304 SS specimens (Ref. 18). As a result, the computational model was modified to include the effect of vaporization and temperature dependent thermal-physical properties. The basic algorithm and the formulation of the governing equations are presented elsewhere (Refs. 16, 18) and will not he repeated here.

Unlike stationary spot GTA welding, in moving arc welds both melting and solidification occur simultaneously. There are two major numerical challenges in modeling moving arc welds and the associated melting and solidification. They are: 1) the heat flow related to absorption and evolution of latent heat, and 2) the fluid flow in the mushy zone.

In the finite temperature range ($T_s < T < T_l$), the latent heat of phase change (L) is defined as a function of the liquid fraction in the mushy zone as

$$f(T) = \begin{cases} L & T > T_l \\ L(1-F_s) & T_l > T > T_s \\ 0 & T < T_s \end{cases}$$

where $F_s(T)$ is the local solid fraction, T_l is the liquidus temperature and T_s is the solidus temperature. The F_s is calculated based on a sigmoidal function as shown in Ref. 15.

The flow in the mushy zone is assumed to follow the Darcy law (Ref. 22) given by,

$$u = -(K/\mu)\,\nabla P$$

where K is the permeability, and μ is the viscosity, such that

u_l	in the liquid
$u = u_l(1-F_s)$	in the mushy zone
0	in the solid

The flow in the mushy region is modeled by using a Darcy source term to modify the momentum equations such that, as the local solid fraction approaches 1, the sources dominate all other terms in the momentum equations and force the predicted velocities to approach values close to zero.

The welding problem was solved using a fixed nonuniform grid system shown in Fig. 2. All simulations were performed using an IBM RS6000 Model 530.

The assumptions made in the present analysis are as follows:

1. Even though thin plates of AISI 304 SS were used in this study, the problem was treated as three-dimensional, with only three layers through the thickness of the specimen.

2. The fluid motion in the weld pool is controlled by buoyancy, electromagnetic and surface tension forces.

3. The power distribution of the heat source is considered as Gaussian, based on available literature (Refs. 9–14).

As in the previous analyses (Ref. 18) of stationary welds, all thermophysical properties were treated as temperature dependent and are given in Fig. 3.

Boundary Conditions

The boundary conditions established were as follows:

1. At the top surface, the heat flux from the arc to the metal surface is specified as a radially symmetric Gaussian distribution.

2. The thermal boundary conditions for atmospheric cooling are formulated in terms of the convective heat transfer and radiative heat transfer. Values of 0.2 for emissivity and 84 W/m²/°C for convective heat transfer coefficient were used in the calculation.

3. Along the solid-liquid interface, the conventional no-slip condition for a viscous fluid was assumed.

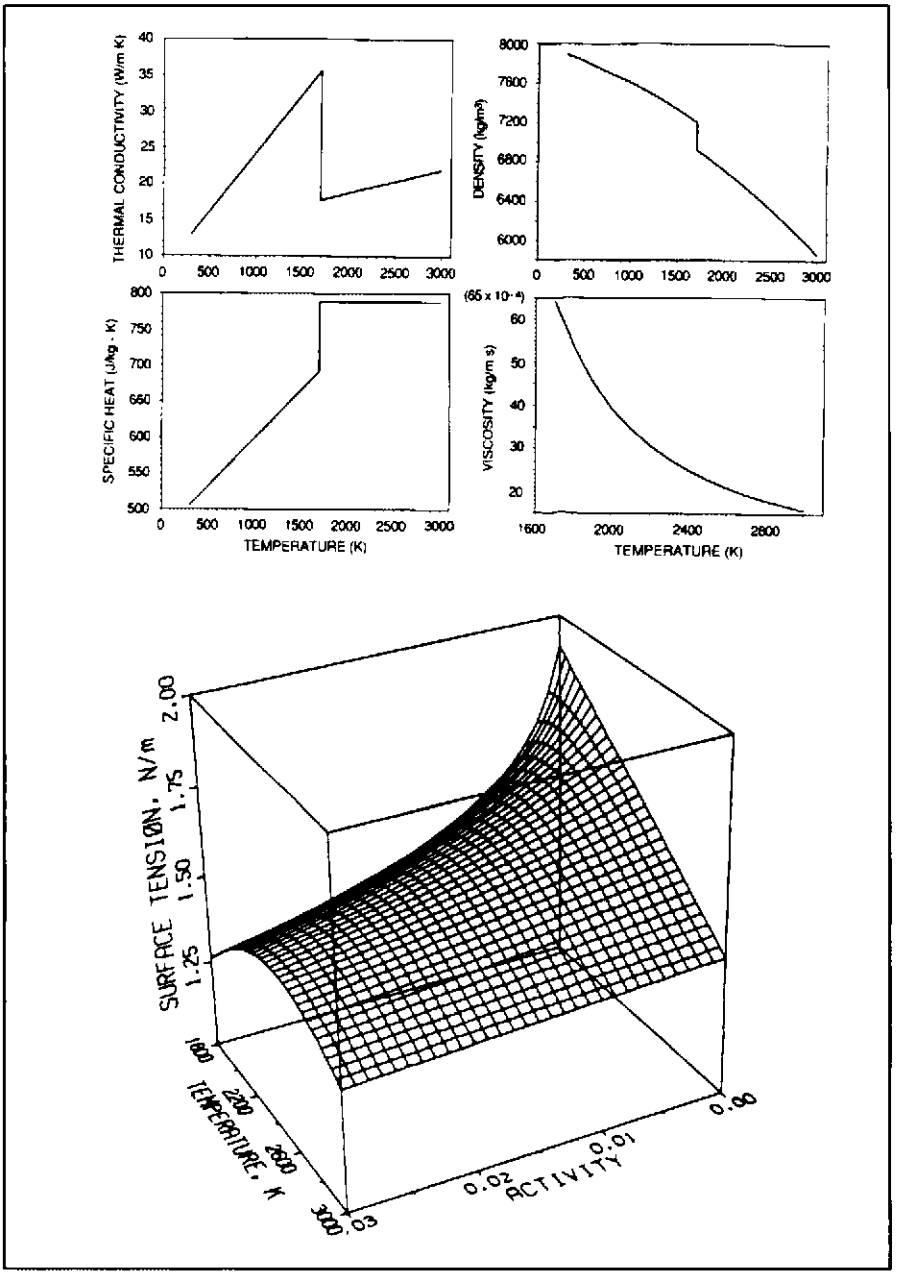

Fig. 3 — Thermophysical properties of Type 304 SS used in the present calculations.

Table 1 — Chemical Composition of 1.5-mm-Thick Type 304 Stainless Steel[23]

	Composition (wt-%)
C	0.06
Co	0.210
Cr	18.13
Cu	0.17
Fe	remainder
Mn	1.68
Mo	0.29
Ni	8.49
P	0.035
S	0.007
Si	0.55
V	0.055

Table 2 — Experimental and Numerical Run Conditions[23]

Case	Voltage (V)	Current (A)	Travel Speed (mm/s)
1	10.1	38	0.423
2	10.1	50	1.270
3	10.1	70	2.540
4	10.1	100	4.230

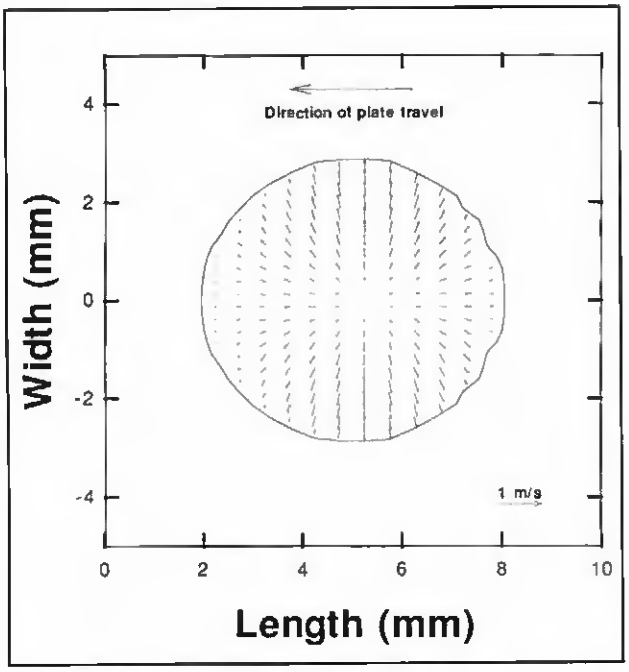

Fig. 4 — Top view of the flow field on the surface of the specimen moving with a constant speed of 0.42 mm/s (1 in./min) in the negative x-direction.

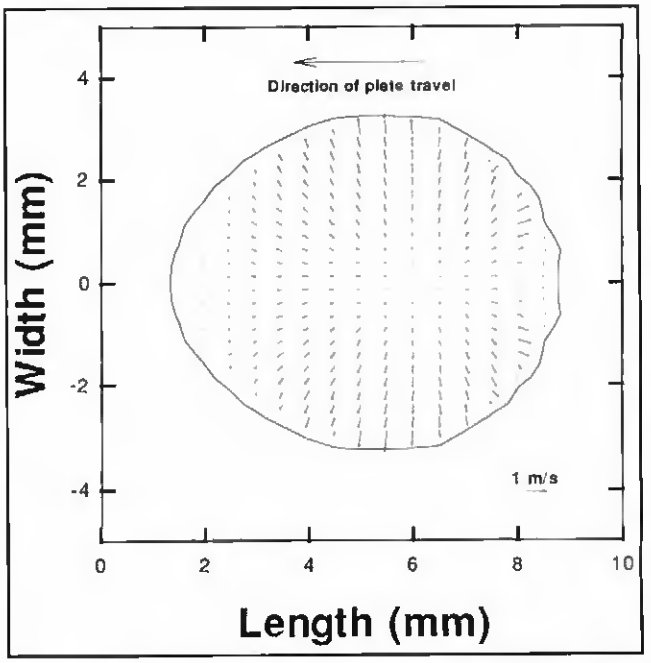

Fig. 5 — Top view of the flow field on the surface of the specimen moving with a constant speed of 1.27 mm/s (3 in./min) in the negative x-direction.

4. A surface tension pressure is exerted on the top free surface due to the directional curvature of the molten metal surface.

5. At the top surface, the shear stress is equated to the gradient of surface tension.

Experimental Procedures

Full penetration autogenous GTA welds were made on 1.5-mm (0.6-in.) 304 SS plates in the horizontal position (Refs. 25, 26). The composition of the material is given in Table 1. The welds were made with an Astromatic E-300-PC pipe-welding machine using a 1/8-in., 35-deg cone angle, 2% Thoriated tungsten electrode. The welding current and duration are entered through digital switches, enabling accurate programming. The electrode arc length was 1.5 mm. Argon cover gas with a flow rate of 18 ft^3/h (38 L/min) was used. The weld pool surface temperatures were measured for four welding speeds ranging from 0.423 mm/s (1 in./min) to 4.23 mm/s (10 in./min).

The optical spectral radiometric/laser reflectance method (Refs. 23–26) was used to obtain extensive measurements of weld pool surface temperatures. The procedures for thermal measurements were described in detail by Kraus (Refs.

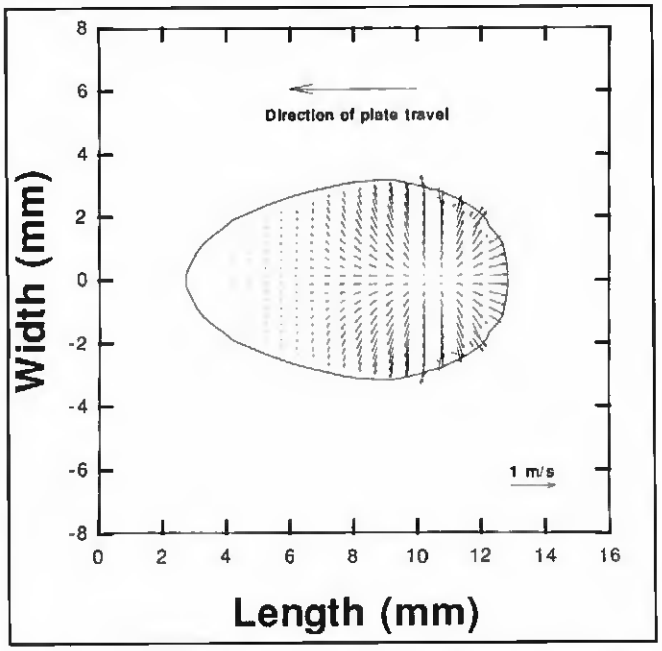

Fig. 6 — Top view of the flow field on the surface of the specimen moving with a constant speed of 2.54 mm/s (6 in./min) in the negative x-direction.

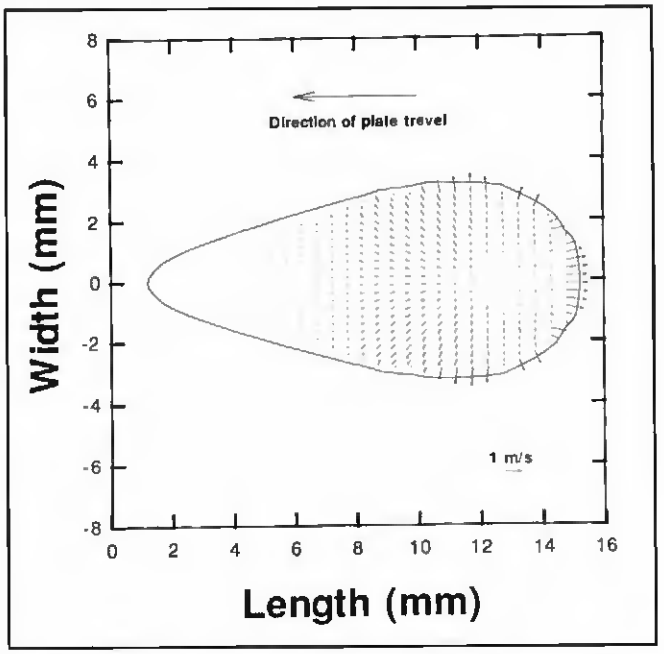

Fig. 7 — Top view of the flow field on the surface of the specimen moving with a constant speed of 4.23 mm/s (10 in./min) in the negative x-direction.

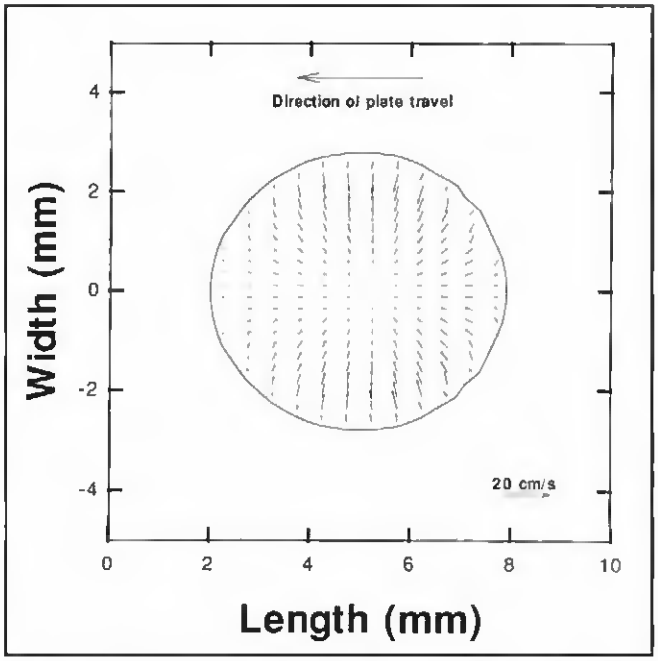

Fig. 8 — Central plane view (horizontal section) of the weld pool flow field for the specimen moving with a constant speed of 0.42 mm/s (1 in./min) in the negative x-direction.

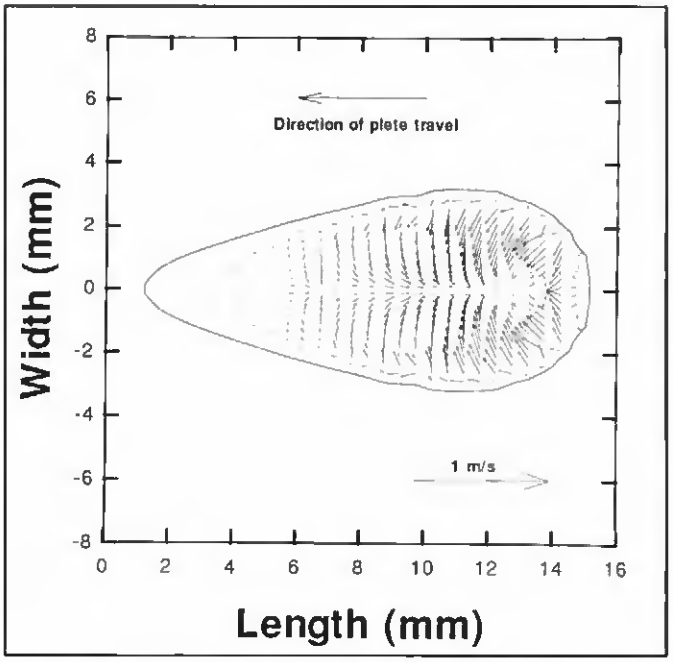

Fig. 9 — Central plane view (horizontal section) of the weld pool flow field for the specimen moving with a constant speed of 4.23 mm/s (10 in./min) in the negative x-direction.

23–26) in earlier publications dealing with surface temperature measurements of GTA weld pools on thin-plate 304 stainless steel. The measurements yield high-resolution, absolute-temperature maps of the weld pool as opposed to the earlier, predominantly uncalibrated, infrared measurements or low-resolution spot measurements.

Following temperature measurements and analysis, selected welds were mounted and polished for optical metallography. Samples were prepared using standard procedures and then etched using HNO_3 and H_2O.

Results and Discussion

The convective heat transfer that occurred during GTA welding of Type 304 SS specimens was numerically analyzed for the various welding speeds considered in this study. Full joint penetration welds were made, with the welding voltage held constant at 10.1 V by adjusting the welding current from 38 to 100 A. Table 2 shows the experimental and numerical run conditions for full joint penetration welding of 1.5-mm-thick 304 SS steel plates. In this section the theoretical results are compared to experimental observations. The theoretical results represent the basic prediction of the model without resorting to any "empirical fine-tuning" of the model. No adjustable parameters were used to achieve a better fit between the predictions and the experimental observations.

Weld pool surface flow patterns for the four cases considered are presented in Figs. 4 to 7. The weld pool surface flows are predominantly outward from the region of peak temperature to the periphery of the weld pool. The predicted flow field suggests that the fluid flow in the weld pool is controlled by the spatial variation of surface tension that exists on the weld pool surface. Since the alloy contains very low levels of surface active elements, a negative surface tension gradient is expected over much of the weld pool surface, explaining the outward flow.

Several earlier experimental (Refs. 13, 27,28) and theoretical (Refs. 11–19) studies have shown that surface tension is the predominant driving force for fluid flow in the weld pool. Most of these earlier studies were for partial and full-penetration welds on relatively thick plates, where the volumetric body force played a very significant role in influencing the overall convective flow. Here in this study, for thin plates, the surface effects are expected to be more dominant because of the higher surface to volume ratio. For full-penetration welding on thin plates, the welding currents used are considerably lower than those typically used for thick plate welding. Consequently, the resulting electromagnetic forces would not be expected to have a pronounced effect on the convective flow. Additionally, buoyancy forces are expected to be negligible since the through-thickness thermal and densimetric gradients are expected to be minimal.

For the cases considered in the present study, the weld pool shape ranged from circular, for a welding speed of 0.423 mm/s, to elongated teardrop shape, for a welding speed of 4.23 mm/s. The maximum flow velocities at the surface ranged from 0.4 m/s at the slowest speed (lowest welding current) to about 1 m/s for the highest welding speed (highest welding current). For all the cases, the calculated maximum velocities were observed at the leading edge of the weld pool where the temperature gradients are expected to be the maximum. At the same time, the flow velocities were considerably lower at the trailing edge of the pool where the temperature gradients are expected to be lower.

It is interesting to note that at the higher welding speeds, the velocities at the trailing edge of the weld pool are extremely small. There has been some speculation that the observed equiaxed structures in some welds may be the result of very high flow velocities in the weld pool, near the solidification front, causing individual dendrites to break and form nucleation sites (Ref. 29). The calculated flow velocities near the trailing edge of the weld pool suggest that it is highly unlikely that such an event can occur, for the conditions investigated, in thin-plate 304 SS.

The strong outward flow at the surface results in an inward flow within the weld pool. This can be clearly seen in Figs. 8 and 9, showing the mid-plane flow pattern for Cases 1 and 4. As would be expected, the resulting inward flow velocities are considerably smaller when compared to the surface flows. The bulk

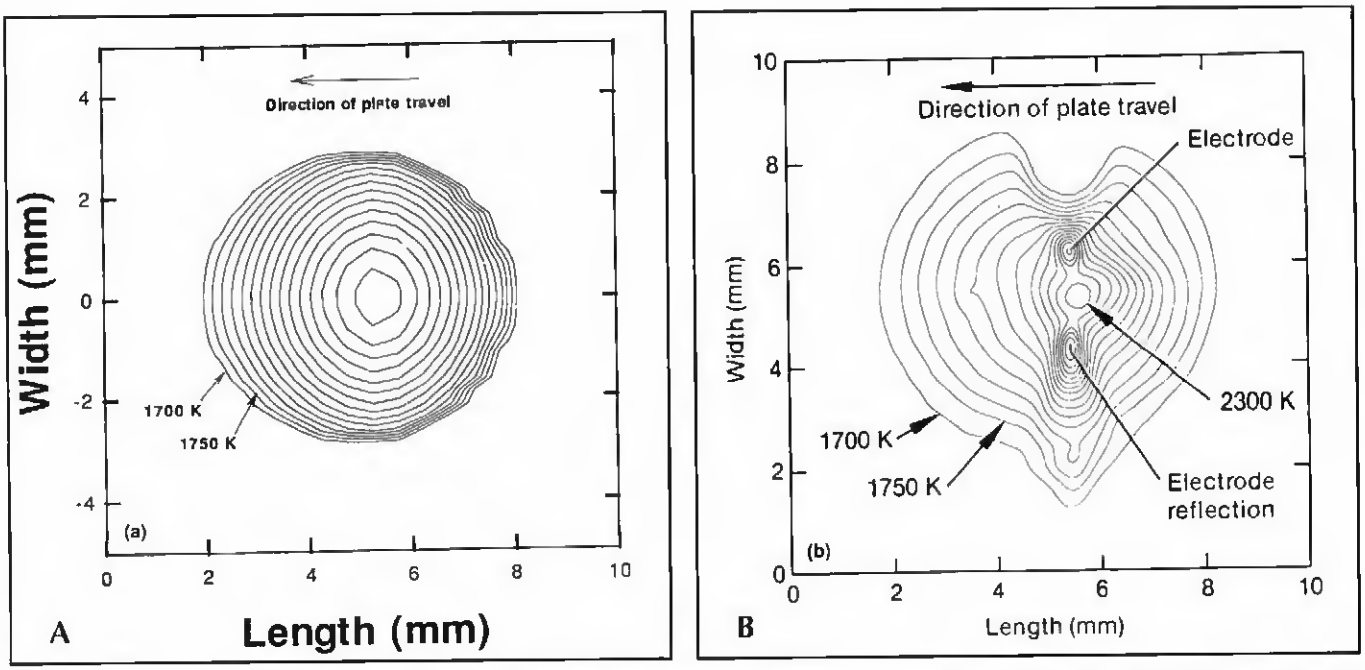

Fig. 10 — Weld pool surface temperature distribution for a specimen moving with a constant speed of 0.423 mm/s (1 in./min) in the negative x-direction. A — experimentally measured; B — calculated.

maximum velocities ranged from 10 to 40 cm/s. Unlike the surface flows, where surface tension controls the fluid flow, the influence of the welding conditions and the weld pool geometry on the flow pattern is clearly visible. For the slow welding speed, the calculated flow pattern indicates a recirculating flow, with the molten metal being transported from the center to the periphery and back. Very little front to back movement of molten metal is observed. On the other hand, for Case 4, a clear front to back flow is observed along the edge of the weld pool. Also, the influence of the weld pool shape on the flow pattern is apparent in Fig. 9. The results show that the predicted size of the weld pool is relatively uniform through the thickness of the plate.

Figures 10 to 13 show the calculated and experimentally obtained weld pool surface temperature contours, in intervals of 50 K, for the four cases considered in this study. Only temperatures equal to or above 1700 K are shown. Evident in the experimental results are the electrode and its spectral reflection in the weld pool. Kraus (Ref. 26) has pointed out that the electrode and its reflection temperatures are not accurate because the electrode emissivity was not measured. Because the electrode temperatures were not of interest, the molten stainless steel

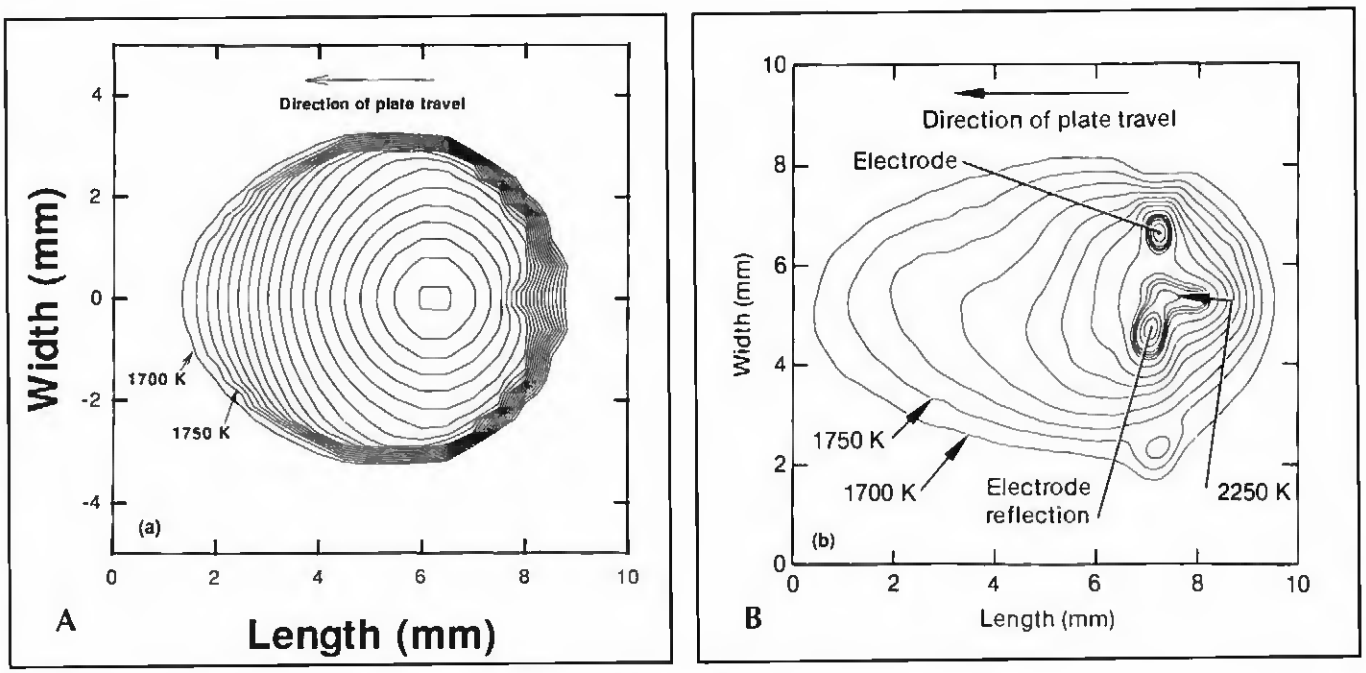

Fig. 11 — Weld pool surface temperature distribution for a specimen moving with a constant speed of 1.27 mm/s (3 in./min) in the negative x-direction. A — experimentally measured; B — calculated.

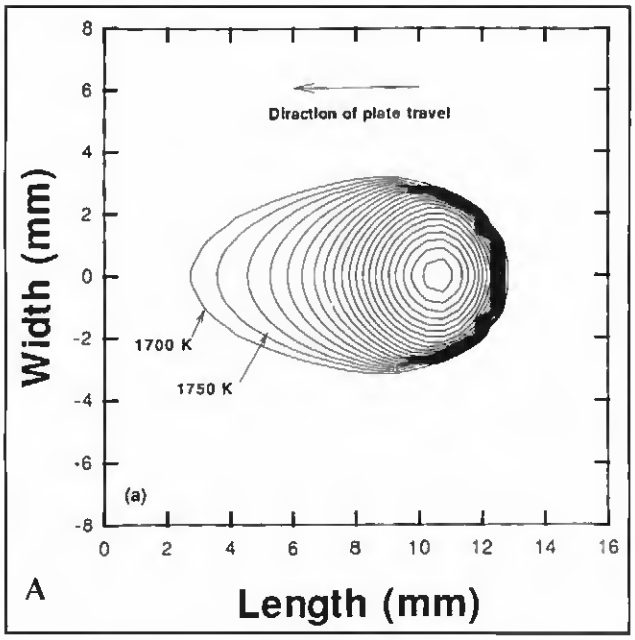

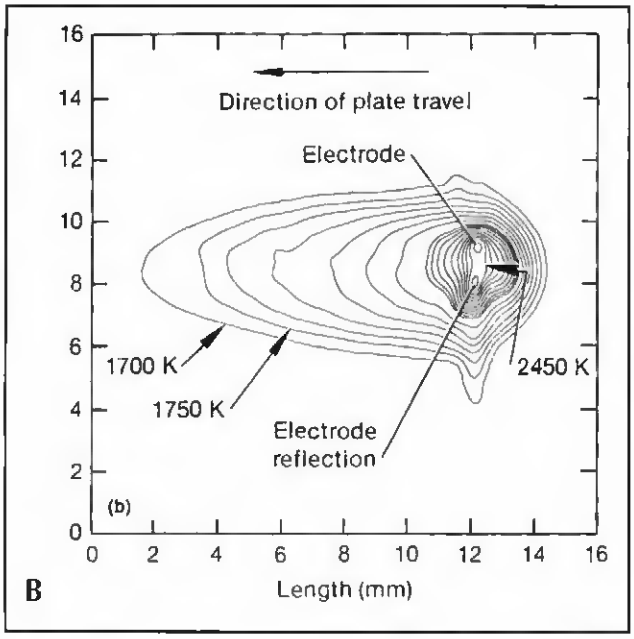

Fig. 12 — Weld pool surface temperature distribution for a specimen moving with a constant speed of 2.54 mm/s (6 in./min) in the negative x-direction. A — experimentally measured; B — calculated.

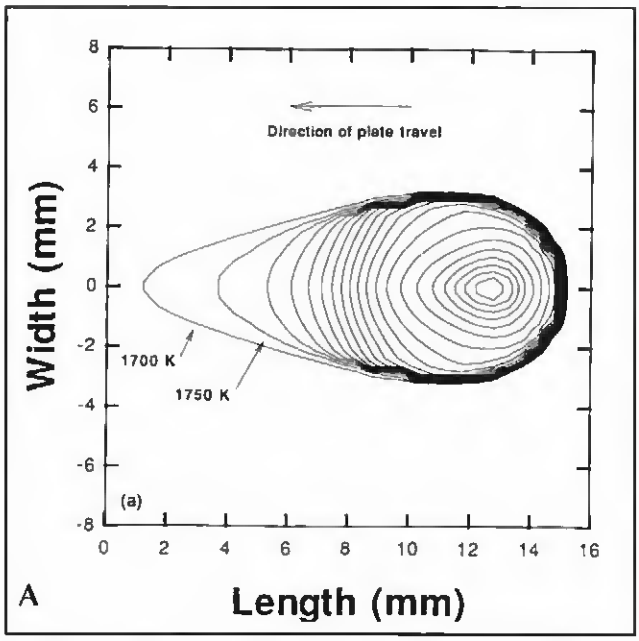

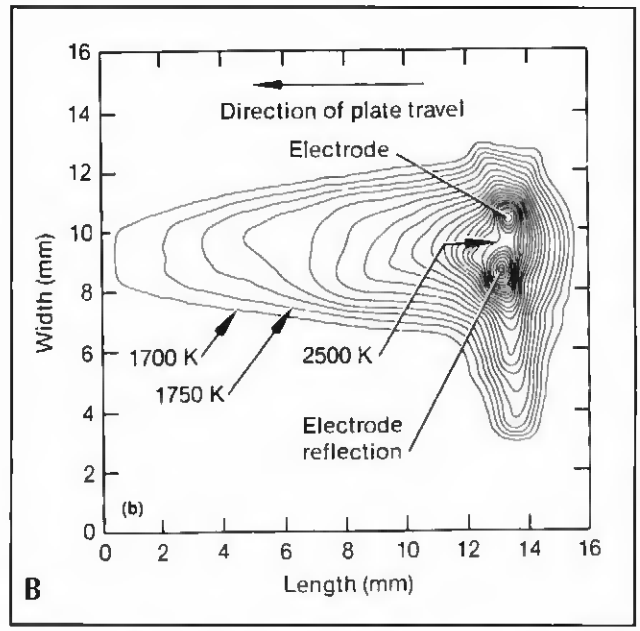

Fig. 13 — Weld pool surface temperature distribution for a specimen moving with a constant speed of 4.23 mm/s (10 in./min) in the negative x-direction. A — experimentally measured; B — calculated.

emissivity was used in these regions.

For Case 1, the calculated peak surface temperature is about 2490 K. Kraus (Ref. 26) made several measurements of weld pool surface temperatures for each of the welding conditions given in Table 2. For Case 1, the measured peak surface temperatures ranged from 2273 to 2335 K. Additionally, for a similar case, an earlier measurement (Ref. 25) using a different power supply and a different heat of 304 SS yielded a peak surface temperature of 2802 K. As the welding conditions are changed from Case 1 to 4, the results show considerable change in the temperature distribution and the peak temperature. For the welding conditions investigated, the calculated peak temperatures ranged from 2490 to 2822 K.

Comparison of the calculated and experimental peak surface temperatures indicate good agreement. It must be pointed out that the calculated temperatures were obtained at the instant of arc shutoff, whereas the experimental measurements were made 3 to 4 ms after arc shutoff. It is of interest to know how much the peak surface temperature drops during this arc decay time. The computational model was used to calculate the temperature drop, 3.6 ms after arc shutoff. The calculated drop of 40 K is in good agreement with the estimates based on experimental results. Kraus estimated this drop by extrapolating the peak surface temperature back to the instant of arc shutoff. His study indicated a drop of approximately 35 to 50 K during the 3 to 4 ms arc decay time.

The dependence of maximum weld pool temperature on heat input is presented in Fig. 14. The heat input is defined as

$$Q = EI/v$$

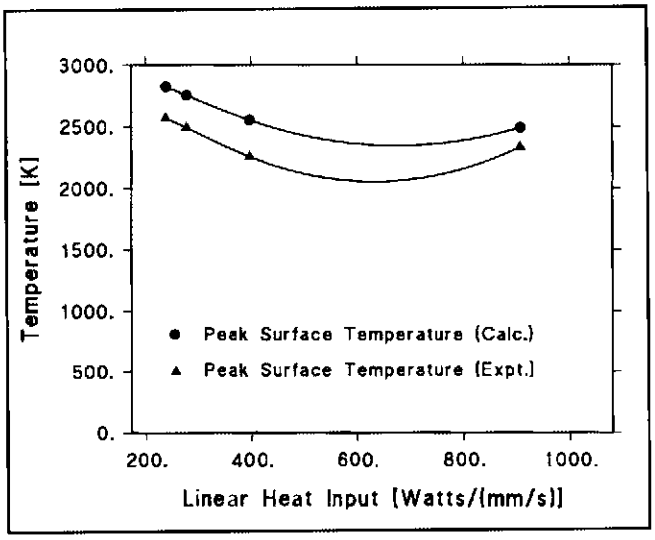

Fig. 14 — Maximum weld pool surface temperature as a function of linear heat input.

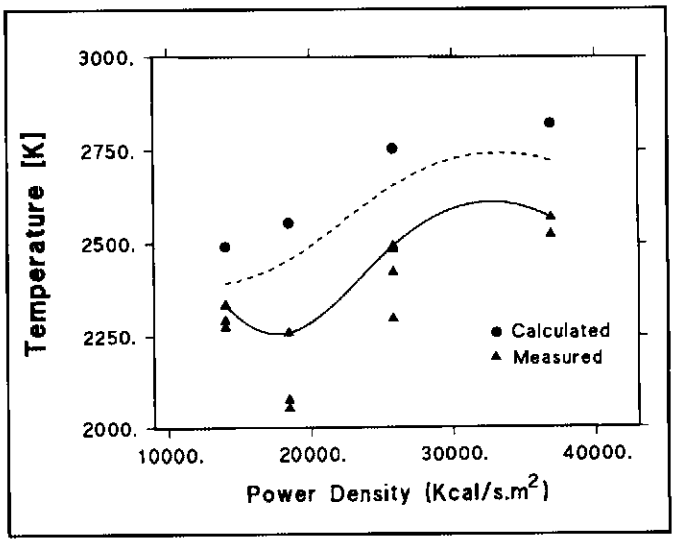

Fig. 15 — Maximum weld pool surface temperature as a function of power density.

where Q is the heat input, E the arc voltage, I the arc current and v the welding speed. Contrary to expected behavior, the weld pool peak temperatures exhibit an inverse relationship with heat input. The experimentally measured values also exhibit similar behavior with heat input. The same results are presented in Fig. 15 as a function of power density. From Fig. 15, the peak temperatures show a much better correlation with the changes in power density, suggesting that the peak surface temperature is primarily controlled by the power density. This should not be surprising, since very high peak temperatures are obtained for low power laser beam welding, where the heat inputs are considerably lower than the conventional welding process.

From Fig. 15, it is apparent that the peak surface temperatures exhibit a nonlinear relationship with welding current. In addition, the experimentally measured peak temperatures initially decreased before increasing with increasing welding current. Kraus (Ref. 25) speculated that changing weld pool convective characteristics could perhaps explain the observed deviation from expected proportional relationships. Indeed, the numerical results presented earlier show some differences in the surface flow patterns and velocities. However, there are no obvious anomalies in the convective flow that can explain the observed nonlinear behavior of the peak surface temperature. It is conceivable that the observed nonlinearity reflects the dynamics between the heat input (power density) into the weld pool and the heat removal from the weld pool due to convective and conductive heat transfer.

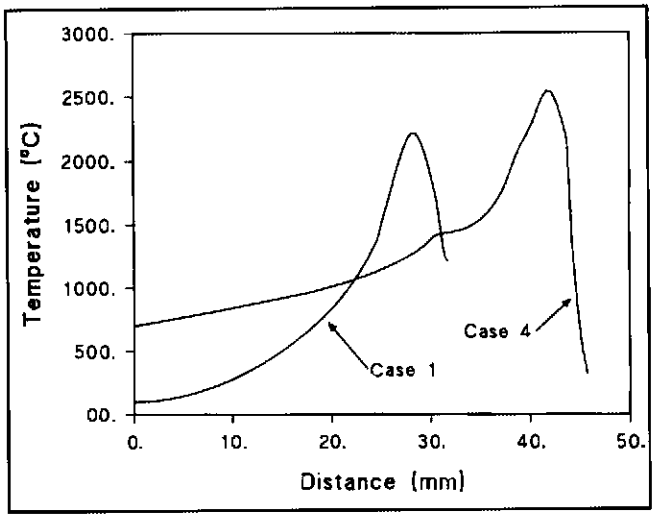

Fig. 16 — Surface temperature profiles for Case 1 and Case 4 taken from left to right through the weld centerline.

The calculated weld centerline surface temperatures are presented in Fig. 16 for welding speeds of 0.423 and 4.23 mm/s. In addition to the difference in peak temperatures, noted earlier, the results show significant differences in the temperature gradients for the two cases, which can influence the solidification structure within the fusion zone. At the higher welding speed, the temperature gradient at the trailing edge of the pool is relatively shallow, which can influence the solidification structure within the fusion zone. Additionally, the relatively flat temperature gradients, which control Marangoni convection, can explain the limited flow velocities at the trailing edge of the weld pool for the higher welding speeds. The results also show that the temperature gradient (dT/dx) behind the weld pool is steeper for the weld made using the lower welding speed.

Figure 17 shows the top surface view of the weld overlaid with the calculated weld pool shape for the slowest welding speed. The macrograph shows a relatively circular weld pool similar to the predicted weld pool shape. Usually, such circular welds are associated with stationary welds. Here, in this case, the slow translation speed of the specimen with respect to the welding arc produced the circular weld pool shape. Comparison between the calculated and experimental weld pool geometry shows excellent agreement. A similar comparison was made for Case 4 and is shown in Fig. 18. The agreement in this case is not as good as Case 1 and represents the worst case of the four.

Conclusions

A multidimensional computational model was used for the analyses of heat and fluid flow during thin-plate full joint penetration welding. The model considers the solid plus liquid mushy zone as a porous media in the calculation of convective heat transfer. The computational model was used to predict the heat flow

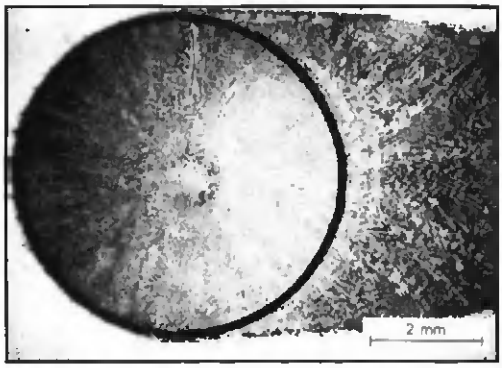

Fig. 17 — Comparison between the computed (sketch overlay) and the observed weld pool geometry for Case 1.

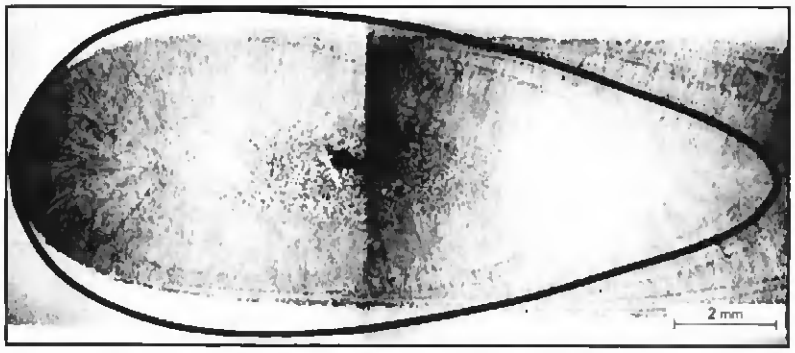

Fig. 18 — Comparison between the computed (sketch overlay) and the observed weld pool geometry for Case 4.

and fluid flow that occur during full-penetration welding of thin-plate stainless steel. The welding parameters were chosen such that the predictions of the model could be correlated with the results of an earlier experimental investigation of weld pool surface temperatures. The predictions of the weld pool surface temperatures, the weld pool size and shape were compared to the corresponding experimental measurements.

The calculated surface flows indicate that the weld pool fluid flow is controlled by the spatial variation of surface tension, particularly for thin-plate full joint penetration welds. The maximum calculated surface velocities ranged from 40 to 100 cm/s. The bulk velocities were considerably lower, ranging from 10 to 40 cm/s. The results showed that for higher welding speeds, the temperature gradients at the trailing edge of the weld pool are very small, resulting in negligible flow velocities. The relatively stagnant region at the trailing edge of the pool can have important consequences on the weld solidification structure.

In general, both computational and experimental studies indicate that the weld pool peak temperature increases with welding current. However, there does not appear to be a direct correlation between the peak surface temperature and the welding current. The calculated peak surface temperatures ranged from 2490 to 2820 K for the conditions investigated. This is in reasonable agreement with experimental measurements.

The calculated weld pool shapes were compared with the macrographs of the terminal shape of the weld pool suggesting reasonable agreement. Excellent agreement was obtained for the slow welding speed. For the highest welding speed the agreement was not as good.

Acknowledgments

The authors would like to thank G. L. Bell and J. C. Whitson of Oak Ridge National Laboratory for reviewing the manuscript. The research was sponsored by the Division of Materials Science, United States Department of Energy, under contract DE-AC05-84OR21400 with Lockheed Martin Energy Systems, Inc.

References

1. Rosenthal, D. 1941. Mathematical theory of heat distribution during welding and cutting, *Welding Journal*, 20: 220-s to 234-s.

2. Adams, C. M. 1958. Cooling rates and peak temperatures in fusion welding, *Welding Journal* 37(5): 210-s to 215-s.

3. Friedman, E. 1978. *Weld Journal* 57: 161-s to 166-s.

4. Ishizaki, K., Murai, K., and Kanbe, Y. 1966. Penetration in arc welding and convection in molten metal. International Institute of Welding Document 212-77-66.

5. Jhaveri, P., Moffat, W. G., and Adams, C. M. 1962. The effect of plate thickness and radiation on heat flow in welding and cutting, *Welding Journal* 41(1): 12-s to 16-s.

6. Hess, W. F., Merrill, L. L., Nippes, E. F., and Bunk, A. P. 1943. The measurement of cooling rates associated with arc welding and their application to the selection of optimum welding conditions, *Welding Journal* 22: 377-s to 422-s.

7. Nippes, E. F., Merrill, L. L., and Savage, W. F. 1949. Cooling rates in arc welds in 1/2 in. plate. *Welding Journal* 28: 556-s to 564-s.

8. Athey, D. R. 1980. A mathematical model for fluid flow phenomena in weld pools. *Journal of Fluid Mechanics* 98: 787.

9. Oreper, G. M., and Szekely, J. 1984. Heat and fluid flow phenomena in weld pools. *Journal of Fluid Mechanics* 147: 53.

10. Tsai, N. S., and Eagar, T. W. 1984. *Modeling of Casting and Welding Process II*, p. 317. Eds. J. A. Dantzig and J. T. Berry, The Metallurgical Society of AIME, Warrendale, Pa.

11. Kou, S., and Sun, D. K. 1985. Fluid flow and weld penetration in stationary arc welds. *Metall. Trans.* Vol. 16A, p. 203.

12. Kou, S., and Wang, Y. H. 1986. Weld pool convection and its effect. *Welding Journal* 65(3): 63-s.

13. Sundell, R. E., Correa, S. M., Harris, L. P., Solomon, H. D., Wojcik, L. A., Savage, W. F., Walsh D. W., and Lo, G-D. 1986. Minor element effects on gas tungsten arc weld penetration. GE Report No. 86SRD013, 1986.

14. Kraus, H. G. 1986. *Journal of Heat Transfer* 108: 591.

15. Zacharia, T., Eraslan, A. H., and Aidun, D. K. 1988. *Welding Journal* 67(1): 18-s.

16. Zacharia, T., Eraslan, A. H., Aidun, D. K., and David, S. A. 1989. *Metall. Trans.* B, (208): 645.

17. Zacharia, T., David, S. A., Vitek, J. M., and DebRoy, T. 1989. *Welding Journal* 68(12): 499-s.

18. Zacharia, T., David, S. A., Vitek, J. M., and Kraus, H. G. 1991. *Metall. Trans.* B, (22B): 243.

19. Choo, R. T. C., and Szekely, J. 1991. *Welding Journal* 70(9): 223-s.

20. Sahoo, P., and DebRoy, T. 1987. *Metall. Trans.* B. 188: 597.

21. Zacharia, T., Vitek, J. M., Goldak, J. A., DebRoy, T., Rappaz, M., and Bhadeshia, H. K. D. H. 1995. Modelling simulation. *Mater. Sci. Eng.* 3: 265.

22. Kurz, W., and Fisher, D. 1990, *Fundamentals of Solidification* 2nd Edition, Lebanon, N.H., Trans. Tech.

23. Kraus, H. G. 1986. Optical spectral radiometric method for measurement of weld-pool surface temperatures. *Optics Letters* 11(12): 773–775.

24. Kraus, H. G. 1987. Optical spectral radiometric/laser reflectance method for noninvasive measurement of weld pool surface temperatures. *Opt. Eng.* 26(12): 1183–1190.

25. Kraus, H. G. 1987. Experimental measurement of thin plate 304 stainless steel GTA

weld pool surface temperatures. *Welding Journal* 66(12): 353-s to 359-s.

26. Kraus, H. G. 1989. Surface temperature measurements of GTA weld pools on thin-plate 304 stainless steel. *Welding Journal* 68(3): 84-s to 91-s.

27. Heiple, C. R., and Roper, J. R. 1982. *Welding Journal* 61: 97-s.

28. Heiple, C. R., and Roper, J. R. 1982. Mechanism for minor element effect on GTA fusion zone geometry. *Welding Journal* 61(4): 97-s.

29. David, S. A., and Vitek, J. M. 1989. Correlation between solidification parameters and weld microstructures. *International Materials Reviews* 34(5): 213–244.

INTERPRETIVE REPORT ON DYNAMIC ANALYSIS AND TESTING OF PRESSURIZED COMPONENTS AND SYSTEMS — FIFTH EDITION

J. S. LEUNG, G. A. ANTAKI, T. L. WANG, R. D. BLEVINS, K. M. VASHI, AND M. S. WHITT

Dynamic analysis of pressurized components is a key element in satisfying specified safety and economical requirements in the design process. Recognizing this, PVRC initiated work to establish needs and priorities, recommend research programs, and help direct research activities toward industrial applications.

A series of interpretive reports has been issued to record the progress and results of this work: WRC Bulletin 246, 1979; WRC Bulletin 269, 1981; WRC Bulletin 303, 1985; and WRC Bulletin 336, 1988.

This Bulletin, the fifth in the series, summarizes the advances made since 1988 and presents new technical issues involving dynamic stress criteria, pressure transients, fluid-structure interaction, seismic analysis, and dynamic restraints. Intended to be a generic guide to future research, it recommends and prioritizes specific research topics which reflect the current as well as the future research needs of industry.

Publication of this document was sponsored by the Committee on Dynamic Analysis and Testing of the Pressure Vessel Research Council.

The price of WRC Bulletin 393 (July 1994) is $40 per copy plus $5 for U.S. and Canada, and $10 for overseas postage and handling. Orders should be sent with payment to Welding Research Council, 345 E. 47th St., Room 1301, New York, NY 10017; (212) 705-7956; FAX (212) 371-9622.